Smart Structures and Systems, *Vol. 36*, *No. 1* (*2025*) *23-38*
https://doi.org/10.12989/sss.2025.36.1.023

2D CNN-based concrete stress monitoring using impedance signals of capsule-like smart aggregate

Quoc-Bao Ta [1a], Ngoc-Lan Pham [1b], Quang-Quang Pham [2c] and Jeong-Tae Kim*[1]

[1] *Department of Ocean Engineering*, *Pukyong National University*, *45 Yongso-ro*, *Nam-gu*, *Busan 48513*, *Republic of Korea*
[2] *Bridge and Road Department*, *Danang Architecture University*, *Da Nang 550000*, *Viet Nam*

(*Received May 1*, *2025*, *Revised July 14*, *2025*, *Accepted July 19*, *2025*)

Abstract. This study aims to develop a 2D CNN deep learning model processing electromechanical impedance (EMI) responses of a capsule-like smart aggregate (CSA) sensor for monitoring stress variation in concrete structures. The following approaches are conducted to obtain the objective. Firstly, an overall scheme of the proposed method is presented. An EMI measurement model is theoretically presented for a CSA sensor embedded in a concrete cylinder under compressive loadings. A 2D CNN model is designed to learn and classify stress-sensitive features from CSA's EMI responses. Secondly, a CSA-embedded concrete cylinder is experimentally investigated to record the EMI signals of the cylinder under a series of compressive stress levels. Thirdly, the performance of the 2D CNN model is investigated for noise-contaminated data sets as well as untrained stress-EMI scenarios. Finally, the accuracy of the proposed 2D CNN model is analyzed by comparatively discussing with a well-established 1D CNN model.

Keywords: compressive testing; concrete structure; convolutional neural network; impedance-based method; PZT sensor; smart aggregate; stress and damage monitoring

1. Introduction

Concrete structure undergoes local damage or degradation during service life. Therefore, it is essential to monitor stress level and damage status in the structure as a pre-requisite process to avoid the risk of major failure induced by the local damage (Khan *et al*. 2020, Smolana *et al*. 2021).

Various non-destructive testing (NDT) methods have been proposed for stress and damage monitoring in concrete structures, including X-ray scanning (Suzuki *et al*. 2017), fiber-optic sensors (Tan *et al*. 2021), strain gauge sensors (Sun *et al*. 2020), cement-based sensors (Lee *et al*. 2020), and vibration-based approaches (Pham *et al*. 2024, 2025). Among these, strain gauges are widely used due to their high accuracy in capturing static or slowly varying stress states. However, they typically require complex wiring, are sensitive to environmental factors, and have limited effectiveness in dynamic conditions. The EMI technique has recently been popular because of its benefits in high sensitivity to dynamic stress changes, fast response over a wide frequency range, and dual functionality as both actuator and sensor. It is also cost-effective and easy to integrate into concrete structures (Na and Baek 2018). The method utilizes PZT sensors to interact with structures, providing information about the local characteristics of the examined area (Liang *et al*. 1994). Surface-mounted PZT sensors could detect local damage but were less sensitive to inner concrete damage (Lim *et al*. 2016, Narayanan *et al*. 2018). Song *et al*. (2008) developed an EMI-based smart aggregate (SA) technique to reduce the effect of noisy ambient conditions and temperature variation on PZT sensors. The SA sensors have been applied to monitor strength development, compressive stress, and internal damage in concrete structures (Pham *et al*. 2021a, b, Li *et al*. 2023). Pham *et al*. (2022) proposed a new SA technique, so-called capsule-like smart aggregate (CSA), with pre-determined frequency ranges for EMI response sensing. The EMI signals recorded from the CSA sensors could directly represent the change in concrete stress as well as the occurrence and development of local damage near the sensors.

The main issues for the SA-based structural health monitoring involve managing the multiple stages of data collection, processing the collected information, and accurately assessing the occurrence and severity of structural damage. So far, the EMI features such as root-mean-square deviation (RMSD) and cross-correlation deviation (CCD) have been commonly utilized for estimating stresses and identifying damage severities in structures. However, the conventional multi-step process requires the rigorous process of feature extraction to guarantee the accurate estimation of stress and damage quantitatively (Sun *et al*. 1995, Zagrai and Giurgiutiu 2001). False damage alerts could be led by the biased selection of EMI features mainly due to insufficient analyses and wrong decisions influenced by human

---

*Corresponding author, Ph.D., Professor,
E-mail: idis@pknu.ac.kr
[a] Ph.D., E-mail: qb.tabao@gmail.com
[b] Ph.D. Student, E-mail: pnlan@pukyong.ac.kr
[c] Ph.D., E-mail: quangpq@dau.edu.vn

Copyright © 2025 Techno-Press, Ltd.
http://www.techno-press.org/?journal=sss&subpage=7

ISSN: 1738-1584 (Print), 1738-1991 (Online)

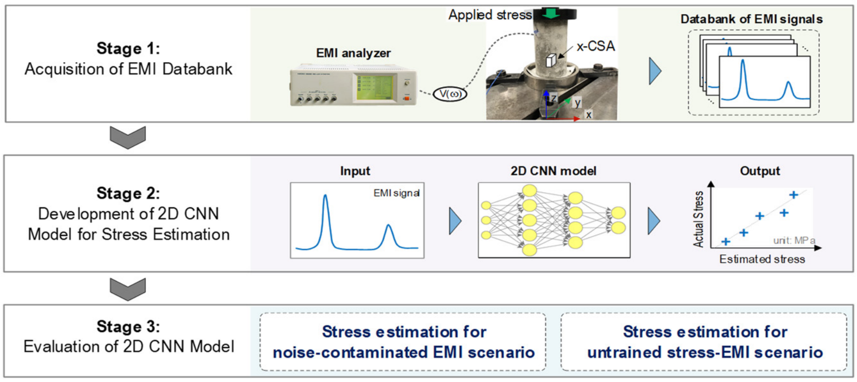

Fig. 1 Scheme of CSA-based concrete stress monitoring via 2D CNN model

interference. As a challenging issue, therefore, the selection of sensitive frequency bands and meaningful EMI features has a critical effect on the accuracy of the estimated results (Park *et al*. 2003, Min *et al*. 2010).

In order to overcome the above-mentioned challenge in the traditional multi-step process, an autonomous process of EMI feature extraction should be implemented for the SA-based damage monitoring. In recent years, deep learning techniques have been effectively employed to assess structural conditions (Abdeljaber *et al*. 2018, Yuan *et al*. 2020, Nguyen *et al*. 2021, 2023). Researchers have integrated CNN-based deep learning algorithms with EMI signals for assessing bolt-loosening status in steel structures (Nguyen *et al*. 2023) and detecting sensor failures (Nguyen *et al*. 2021). A few studies have attempted combining CNN algorithms with EMI techniques to assess the integrity of concrete structures (De Oliveira *et al*. 2018, Ai *et al*. 2022, Nguyen *et al*. 2022). Nguyen *et al*. (2022) developed a 1D CNN model to automatically process and extract features from raw EMI responses for monitoring damage in a pre-stressed reinforced concrete beam. Lately, Ta *et al*. (2024a) designed a 1D CNN deep regression learning model for concrete stress monitoring via processing raw EMI responses measured by the SA sensors. Stresses in SA-embedded concrete cylinders could be automatically estimated with high accuracy, even under noise effects and missing data.

By extracting local patterns along a single dimension, the above-listed research works have demonstrated that 1D CNN was effective for sequential data such as time-series or frequency-series sensor signals. In contrast, 2D CNNs are designed for grid-like data where filters slide across two dimensions to capture spatial relationships and hierarchical features. This spatial capability allows 2D CNNs to preserve the arrangement of features, capture complex patterns, and exploit correlations both within and across channels. Their ability to learn hierarchical features makes them powerful for tasks requiring spatial understanding such as pattern recognition. Leveraging the advantages of 2D CNN for impedance sensor signals is promising for improving both training efficiency and prediction accuracy. In this study, a 2D CNN deep regression learning model is investigated for the CSA sensors to effectively process EMI responses for concrete stress monitoring. The following approaches are implemented to achieve the goal. Firstly, the overall scheme of the proposed method is presented. The 2D CNN model is designed to process CSA's EMI responses for estimating concrete stress. Secondly, the compression experiment on a CSA-embedded concrete cylinder is carried out to record EMI responses under different applied stresses. Thirdly, the performance of the developed model is investigated under the effect of noise-contaminated EMI and untrained stress-EMI scenarios. Finally, the 2D CNN model is comparatively evaluated to the 1D CNN model regarding to learning performance and testing accuracy on stress estimation to demonstrate the effectiveness of the proposed approach.

2. Methodology

2.1 Scheme of CSA-based concrete stress monitoring via 2D CNN model

Fig. 1 illustrates the scheme of CSA-based concrete stress monitoring via 2D CNN model. It has three main stages: acquisition of EMI databank, development of 2D CNN model for stress estimation, and evaluation of 2D CNN model.

In the first stage, a databank is constructed for stress estimation by acquiring raw EMI signals and their matching structural conditions (e.g., stress levels and damage severities) of CSA sensors embedded in concrete cylinders. In the second stage, a 2D CNN model is designed for extracting hidden features of the collected EMI signals and deep learning the input EMI features corresponding to the output stress values. The accuracy of the CNN model is evaluated by comparing the estimated output values with the actual values. In the final stage, the performance of the 2D CNN model is evaluated for two practical situations of the CSA-embedded concrete structure. At first, the accuracy of stress estimation is evaluated for noise-contaminated EMI scenarios. Next, the accuracy of stress estimation is evaluated for untrained stress-EMI scenarios.

2.2 CSA-based EMI technique

Fig. 2 shows the scheme of the CSA-based EMI concrete stress monitoring technique. The technique allows monitoring of EMI responses via CSA sensors embedded in concrete structures. The structural design of the capsule-like

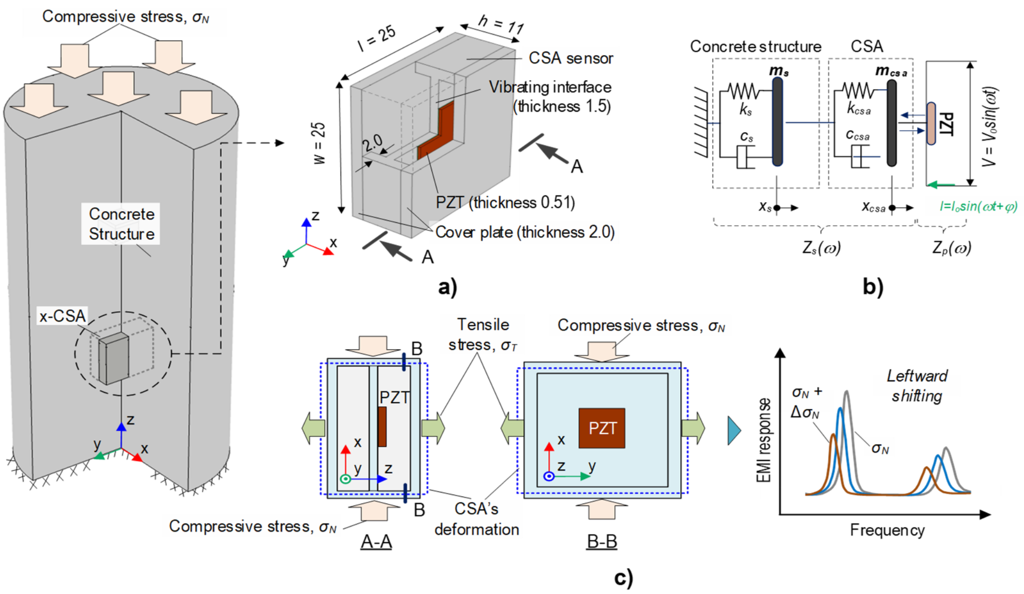

Fig. 2 CSA-based EMI concrete stress monitoring technique: (a) CSA sensor; (b) 2-DOF impedance model; (c) Behavior of CSA sensor embedded in concrete structure under compression

smart aggregate (CSA) sensor allows it to operate effectively in multiple directions. The directional sensitivity has been verified in our recent studies (Pham *et al.* 2022, Ta *et al* 2024b, c), which evaluated CSA performance under both axial and lateral stress conditions.

Fig. 2(a) shows a CSA sensor oriented to the x-axis (x-CSA) in the concrete cylinder. The x-CSA sensor is formed by assembling a vibrating interface (21 × 21 × 1.5 mm) extended wall frame thickness of 2 mm and two aluminum cover plates (25 × 25 × 2 mm) (Pham *et al.* 2022). In the interface, a PZT patch (10 × 10 × 0.51 mm) is surface-mounted in the middle of the vibrating interface. The PZT interface is designed to sense its flexural vibration responses with respect to the PZT sensor's deformation along the x-axis. The cover plates aim to protect the PZT sensor and vibrating interface during concrete curing.

The capsule-like smart aggregate (CSA) offers several key advantages over surface-mounted PZT sensors. The vibrating interface enables frequency control and sensitivity, enabling more consistent signal interpretation. The aluminium capsule provided strong mechanical protection, reducing the risk of damage during construction. Being embedded within the concrete allowed CSA to couple with internal stress zones and improve sensing accuracy. The CSA sensors cannot be easily replaced after installation; however, the performance of the embedded PZT is ensured by the capsule structure.

As shown in Fig. 2(b), the 2-DOFs impedance model represents the coupling system of the CSA and concrete structure (Pham *et al.* 2022). The inverse piezoelectric effect converts electrical energy into mechanical energy. Due to inverse piezoelectric effect, and input harmonic voltage induces a deformation of PZT. At the same time, the electric current is measured and then it is used to calculate the EMI. The EMI Z(ω) is a function of the structural-mechanical impedance of the PZT sensor and that of the CSA-concrete structure

$$Z(\omega) = \frac{V}{I} = \left[i\omega \frac{\omega_p l_p}{t_p} \left(\hat{\varepsilon}_{33}^T - \frac{1}{Z_p(\omega)/Z_S(\omega) + 1} d_{31}^2 \hat{Y}_{11}^E \right) \right]^{-1} \tag{1}$$

where the variables w_p, $t_{p,}$ and l_p is the dimensions of the piezoelectric patch in terms of width, thickness, and length, respectively; $\hat{\varepsilon}_{33}^T$ denotes the complex dielectric constant of at zero stress; $Z_S(\omega) = \hat{Y}_{11}^E w_p t_p/(j\omega l_p)$ represents the structural-mechanical impedance characteristics of PZT; d_{31} represents the PZT's constant in one direction at zero stress; $\hat{Y}_{11}^E$ is Young's modulus of the PZT sensor under the field condition at the zero electric. It is clear that the EMI's real part, $Z(\omega)$, contains both the structural-mechanical impedance of the PZT patch ($Z_p(\omega)$) and of the CSA-concrete structure ($Z_s(\omega)$), as shown in Eq. (1). When the properties of PZT remain constant, external effects on host structure would affect the impedance responses of the CSA–concrete structure. Thus, the changes in structure characteristics induced by stress or damage could affect the measured EMI signatures.

Fig. 2(c) shows the behavior of the x-CSA sensor embedded in the concrete structure subjected to compressive stress, σ_N. The stress-strain responses occurred in the sensor due to the effect of compressive stress in the concrete structure. Specifically, the x-CSA sensor's vibrating interface is subjected to a compressive deformation in the x-direction (see cut plan A-A). Meanwhile, other surfaces of the x-CSA sensor (i.e., z- and y-directions) tend to expand under tensile stress σ_T induced by the effect of Poisson's rule (see Fig. 2(c)). The expansion of the vibrating plate induced by the tensile stress produces the change in structural impedance which can be measured by EMI responses from the PZT patch in the vibrating plate. The increment of the applied stress on the x-CSA-embedded concrete structure could cause the leftward-shifting trend of EMI responses.

2.3 Databank of EMI signals

2.3.1 Data configuration for noise-contaminated EMI scenarios

EMI signals may undergo changes due to diverse factors like sensor configuration and temperature variation (Jalloh 2005). In order to account for all these variables, comprehensive experiments should be conducted with challenges and expenses. Thus, employing data augmentation emerges as a viable substitute for considering the realistic measurement conditions of the analyzed structure. A prevalent method of data augmentation is to involve Gaussian noise in the recorded EMI signals, as it effectively represents typical electronic and environmental interference and provides a statistically sound basis for testing model robustness.

Fig. 3 illustrates the data configuration for noise-contaminated EMI scenarios. The performance of the 2D CNN-based stress estimation model is evaluated via training, validation, and testing sets generated from the measured impedance-stress databank. For each applied stress level, EMI responses are recorded with four ensembles to assure the signal's reliability in impedance measurement method. To construct the training set, the first two ensembles are added Gaussian noise with standard deviations of 0%, 1%, 2%, 3%, 4%, and 5% of the signal amplitude. The third ensemble is used to track the overfitting status during the training procedure (Salman and Liu 2019). To construct the testing set, noise levels ranging from 1% to 16% are injected into the last ensemble of each stress level, with a 1% increment. Note that Section 4.1 demonstrates the noise-contaminated EMI data and the evaluation of the 2D CNN model

2.3.2 Data configuration for untrained stress-EMI scenarios

A well-designed deep learning model should perform well even when trained with small data (Min *et al*. 2010). However, CNN-based deep learning techniques used to lack of stability and accuracy when they were trained with limited data (Melville *et al*. 2018). Thus, the performance of the 2D CNN model is evaluated for untrained stress-EMI scenarios by reducing the amount of training data in the dataset.

As shown in Fig. 4, the first two ensembles (among four ensembles) are added with noises (with standard deviation from 0% to 5% of signal magnitude) to generate a training dataset for the 2D CNN model. The third ensemble of each applied stress level is utilized to validate the model. The last ensemble of each level is added noises with a standard deviation from 1% to 5% of signal magnitude to construct the testing set. Two scenarios are established to investigate the effect of untrained data on the 2D CNN's performance. In the first scenario, the data for training and validating 2D CNN model, so-called training and validating set 1, is established by excluding the stress level S2 (among eight levels S1-S8). In the second scenario, the data for training and validating the model, so-called training and validating set 2, is established by excluding the stress levels S2 and S4. Note that Section 4.2 demonstrates the untrained EMI-stress data and the evaluation of the 2D CNN model.

2.4 Design of 2D CNN architecture

As shown in Fig. 5, a 2D CNN-based deep learning model was designed to estimate stress-EMI regression of CSA-embedded concrete structures. The architecture of the

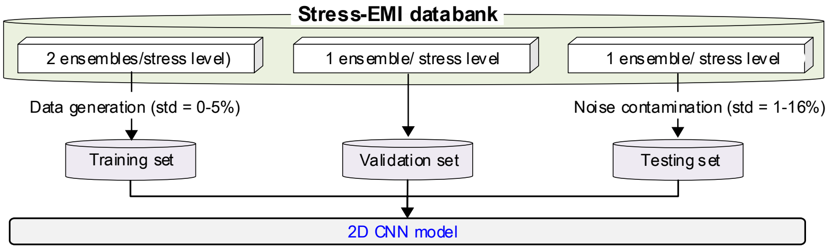

Fig. 3 Data configuration for noise-contaminated EMI scenarios

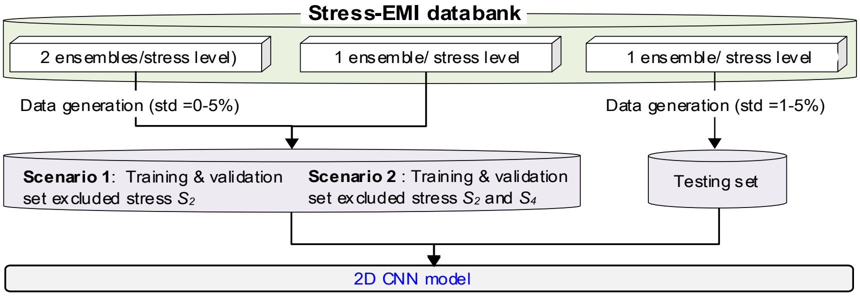

Fig. 4 Data configuration for untrained stress-EMI scenarios

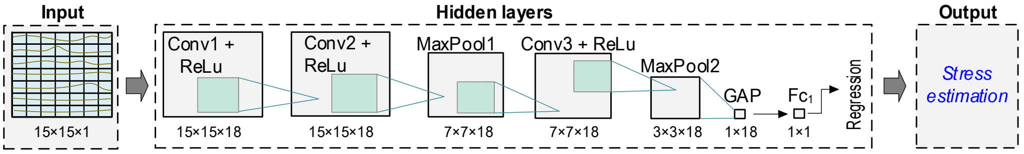

Fig. 5 Architecture of 2D CNN deep learning model using EMI signals measured by CSA sensor

proposed 2D CNN model was built based on the previous well-known model with adjusting hyper-parameters guided by the study (Lecun *et al.* 1998, Zhang and Wallace 2015). As presented in Appendix A, a preliminary study had been conducted to determine a proper architecture. Three variants of the 2D CNN architectures (M1-M3) were investigated and compared in terms of their training efficacy. Based on the comparative analysis, the most effective architecture, M3, was selected for concrete stress estimation.

The 2D CNN architecture includes three parts: an input, hidden layers, and an output. In the 1D CNN approach, the EMI signal—consisting of 225 data points—is input as a one-dimensional array of shape 225 × 1. For the 2D CNN, we reshape this same 225-point signal into a 15 × 15 × 1 matrix. The resulting format allows the 2D CNN model to exploit spatial correlations within the EMI signal, which is not feasible with a purely sequential (1D) approach. Firstly, the input of the 2D CNN deep learning model receives 15 × 15 × 1 (height × width × channel) input data. Each input signal has 225 measurement points within its frequency band.

More information regarding to the measured EMI data can be found in Section 3.3. Secondly, the hidden layers include three Conv layers with three ReLU layers, two Maxpool layers, one global average pooling (GAP) layers (Lin *et al.* 2013), a Fc layer, and a Regression output layer. The total training parameters of the 2D CNN model are 6067 parameters. The layer properties of the 2D CNN layers are described in Table 1. The functionality of Conv, ReLu, and Maxpool layers is found in the study (Goodfellow *et al.* 2016). The GAP layer, followed by the Maxpool layer, is to average feature maps. The Fc layer combines and transforms feature maps into lower-dimensional representations suitable for the Regression layer. Finally, the output from the regression layer will be a stress value estimated in MPa unit.

The loss function in Eq. (2) represents the mean absolute error (MAE) of the regression layer. In the equation, the N signifies the total data, σ_i and σˆ_i (unit in MPa) denote the estimated stress and the actual stress for the ith data. The root mean square error (RMSE) index is calculated by Eq. (3) to evaluate the accuracy of the trained 2D CNN regression model on the testing dataset. The RMSE indicates the estimation error in terms of stress monitoring, by measuring the average of the squares of the errors between the estimated stress and the actual stress. Both the loss and RMSE values have units of MPa. Lower values indicate higher accuracy and better performance of the model in predicting stress.

Table 1 Layer properties of 2D CNN layers

No.	Type	Depth	Filter	Stride	Padding
1	Conv1 + ReLu	18	3 × 3	1	Same
2	Conv2 + ReLu	18	3 × 3	1	Same
3	Maxpool1	-	2 × 2	2	-
4	Conv3 + ReLu	18	3 × 3	1	Same
5	Maxpool2	-	2 × 2	2	-
6	GAP	-	-	-	-
7	Fc1	1	-	-	-
8	Regression	-	-	-	-

$$Loss = \frac{1}{N}\sum_{i=1}^{N}\left|\sigma_i - \hat{\sigma}_i\right| \tag{2}$$

$$RMSE = \sqrt{\frac{1}{N}\sum_{i=1}^{N}(\sigma_i - \hat{\sigma}_i)^2} \tag{3}$$

2.5 Statistical index for damage classification

The CCD and RMSD index can be used as a damage metric index to quantify the change changes in the impedance signals

$$CCD = 1 - \frac{1}{\sigma_Z \sigma_Z^*} E\{[Z_i - \bar{Z}][Z_i^* - \bar{Z}^*]\} \tag{4}$$

$$RMSD(Z, Z^*) = \sqrt{\sum_{i=1}^{N}[Z^*(\omega_i) - Z(\omega_i)]^2 / \sum_{i=1}^{N}[Z(\omega_i)]^2} \tag{5}$$

The alarming threshold is determined by the upper control limit (UCL) as follow

$$UCL = \mu + 3\sigma \tag{6}$$

where E[.] is expectation operation; $Z(\omega_i)$ is the measured impedance signals; (*) denotes the damage state; μ and σ are mean and standard deviation of the damage index dataset.

3. Experimental test

3.1 Fabrication of CSA-embedded concrete cylinder

Fig. 6 shows the fabrication process of a CSA-embedded concrete cylinder. A CSA fabrication process is detailed in a published work (Pham *et al.* 2022). The CSA was placed at the location of a standard plastic cylinder mold (with a size of 100 × 200 mm). One CSA was oriented with the planar surface of the PZT parallel to the applied force under compression, and it was called an x-CSA sensor.

The x-CSA was spaced at a distance of 60 mm from the bottom. Plastic wires and a steel bar (length of 150 mm, ϕ2 mm) were utilized to fix the x-CSA sensor to the cylinder mold. Then, the casting process for the concrete cylinder was conducted with the CSA sensor installed inside. The concrete components were weighted using a digital scale. Then, they were evenly mixed by hand and poured into the cylinder molds. After 48 hours of concrete casting, the molds were removed, and the concrete samples were cured via the wet blankets within 28 days. Table 2 describes the material properties of the CSA-embedded concrete cylinder.

3.2 Experimental setup

Fig. 7 shows the test setup of a CSA-embedded concrete cylinder under compression test. As shown in Fig. 7(a), a concrete cylinder was positioned within the load frame of a servo-hydraulic materials test system (MTS system). A 500 kN capacity load cell was employed to monitor the real compression force. An impedance analyzer, HIOKI 3532, was used to measure EMI signals from the CSA sensors. The room temperature was also monitored via KYOWA EDX-100A during the experiment. Only one concrete cylinder specimen was used in the experiment. Fig. 7(b) shows nine loading scenarios on the cylinder, S0 = 0 MPa to S8 = 15.24 MPa. The MTS multipurpose test software was utilized to control the applied stress levels. Time intervals for stress increase and EMI measurement were 2.5 and 4.5 minutes, respectively. The loading rate for each level was maintained at a consistent velocity of 0.0113 MPa.s-1. The EMI measurements were recorded in the frequency range from 15 kHz to 26 kHz with 224 intervals (i.e., to measure 225 points). The frequency range was predetermined based on the characteristics of the CSA's vibrating plate (Pham *et al*. 2022). Ambient temperature could affect impedance measurements. This issue could be mitigated by collecting data under consistent thermal conditions. In this study, the measured temperature fluctuated between 22°C and 23°C. The temperature effect on the EMI signals might be disregarded. The crack is developed with the increasing in the stress level. No visible cracking was observed in stress levels S_0 to S_7. Cracking was observed only at stress level S_8, corresponding to 0.6fck. The experiment was stopped as soon as the first visible surface crack appeared on the specimen.

3.3 EMI signals

Fig. 8 shows measured EMI responses of the x-CSA sensor under applied stresses $S_{0\text{-}8}$. In each stress level, four EMI measurements (4 ensembles) were recorded in the frequency range of 15-26 kHz. As shown in Fig. 9, an EMI plot (in average of EMI ensembles) was provided for an evaluation relevant to the trends of the resonant frequency peak and real EMI magnitude. It is observed that the resonant peaks expressed the leftward shifting trend, and their corresponding EMI magnitudes were reduced under

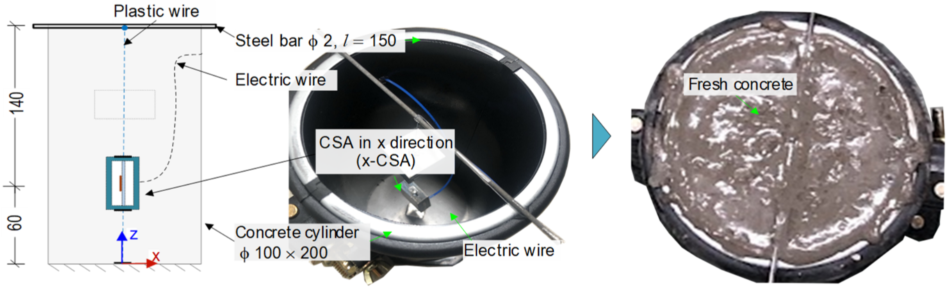

Fig. 6 Fabrication of x-CSA-embedded concrete cylinder (dimensions in mm)

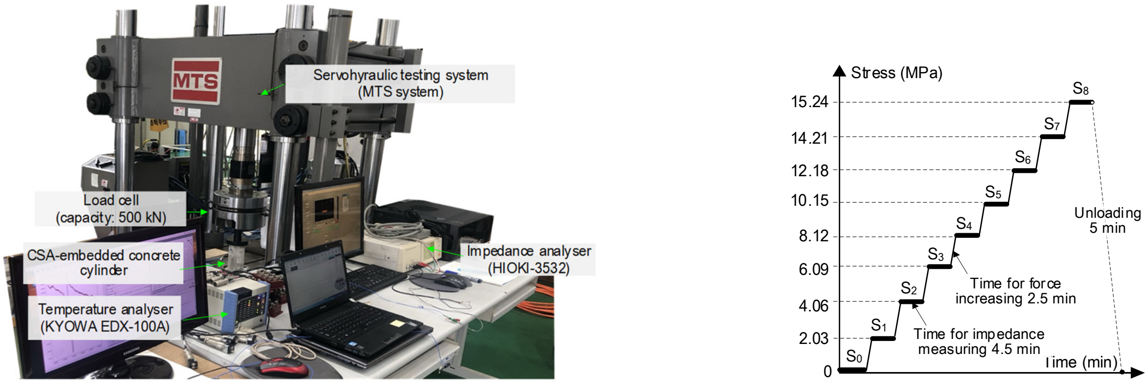

(a) Experimental setup (b) Applied loading history

Fig. 7 Experimental Setup for CSA-embedded concrete cylinder under compression test

Table 2 Material properties for CSA sensor embedded-concrete cylinder

Properties	Aluminum (6061-T6)	PZT 5A	Epoxy layer	Concrete
Mass density, ρ (kg/m^3)	2700	7750	1090	2400
Young's modulus, E (GPa)	68.9	62.1	0.75	25.43
Poisson's ratio, v	0.33	0.35	0.3	0.2
Dielectric loss factor, δ	0.02	0.015	0.02	
Yield strength, σ_y (MPa)	241			
Compressive strength, σ_c (MPa)			32.3	25.3
Damping loss factor, η		0.0125		
Dielectric constant, ε_{33}^T (F/m)		1.53×10^{-8}		
Coupling constant, d_{31} (m/V)		-1.71×10^{-10}		

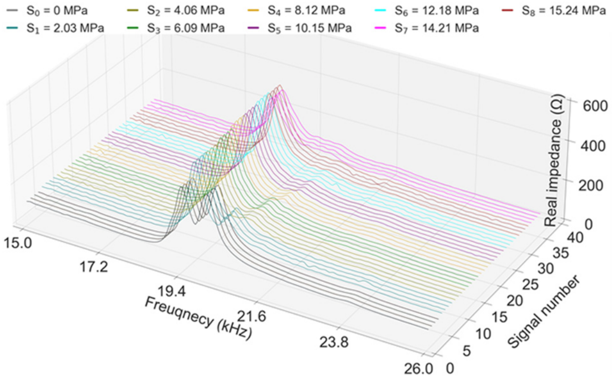

Fig. 8 Measured EMI responses of x-CSA in cylinder under applied stress levels $S_{0\text{-}8}$

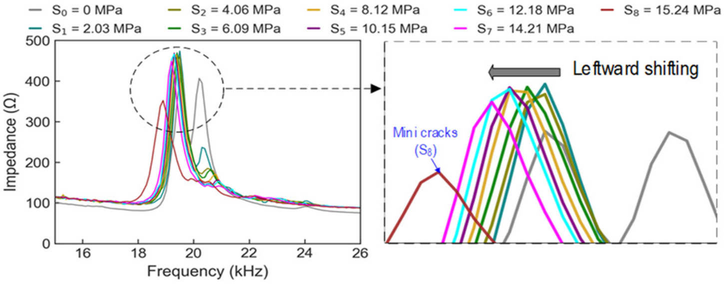

Fig. 9 EMI responses (in average of ensembles) of x-CSA in cylinder under applied stresses $S_{0\text{-}8}$

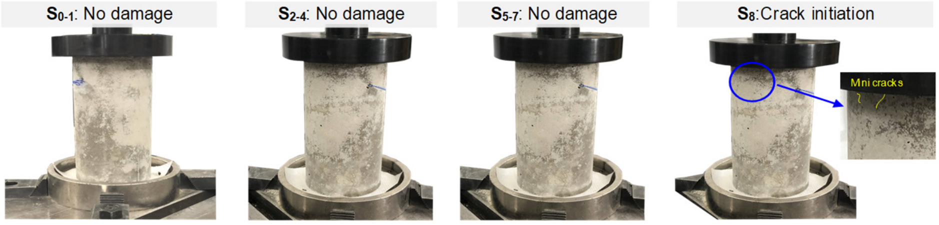

Fig. 10 Visual observation of cylinder during loading steps $S_{0\text{-}8}$

the stress increment. The variation trend of the experimental EMI signals was consistent with the theoretical explanation in Section 2.2. Fig. 10 shows the observation of cylinder during loading steps $S_{0\text{-}8}$, visually checking damage status on the cylinder. Crack initiation was found at the stress level S_8.

3.4 Statistical quantification of EMI responses

EMI features (RMSD and CCD (Nguyen et al. 2022)) were calculated from the measured EMI data of the x-CSA-embedded concrete cylinder under compressive tests. The first stress level S_0 (at 0 MPa) was neglected in EMI feature

(a) RMSD

(b) CCD

Fig. 11 EMI features of x-CSA sensor under applied stresses ($S_{1\text{-}8}$)

computation due to the uncertainty effect in experimental measurements. To assist decision-making, the upper control limit (UCL) was calculated from three standard deviations from the mean, corresponding to a 99% confidence level. The quantified index exceeding the UCL threshold signified changes under the applied stress level. The error bars, which represented the standard deviation of the EMI ensembles, were also plotted.

Fig. 11 shows the EMI features of the x-CSA sensor under applied stresses ($S_{1\text{-}8}$). The RMSD indices linearly increased with increasing stress levels from S_2 to S_7 (see Fig. 11(a)). The RMSD index suddenly changed at the stress level S_8. The magnitudes of CCD indices non-linearly increased under increasing stress levels (see Fig. 11(b)). It is observed that a sudden shift was occurred at stress level S_8 by the RMSE and CCD indices, indicating the formation of internal and surface cracks (Pham *et al*. 2021a, Kocherla *et al*. 2021).

After analyzing the statistical metrics, it is observed that both RMSD and CCD indices exhibited high sensitivities to variations in applied stress levels. Although the mentioned statistical indies could quantify damage to concrete structures, it required multi-steps of data processing and could not be automated for stress estimation. Therefore, there existed a need to develop an automated stress estimation technique.

4. Evaluation of 2D CNN model

4.1 Stress estimation for noise-contaminated EMI scenarios

4.1.1 Data preparation

Following the data configuration scheme described in Fig. 3, the databank of the measured stress-EMI signals of the concrete cylinder was formed for the 2D CNN deep regression learning model. Table 3 shows eight labels of “stress” which were assigned to the datasets. The first seven stress levels (S_1 - S_7) were labeled for EMI data under stress values from 2.03 MPa to 14.21 MPa with an increasing interval of 2.03 MPa orderly. The eighth level (S_8) was labeled for 15.24 MPa.

Table 3 Data labeling for stress estimation

Stress level	Observation	Labeled stress (MPa)
S_1	No damage	2.03
S_2	No damage	4.06
S_3	No damage	6.09
S_4	No damage	8.12
S_5	No damage	10.15
S_6	No damage	12.18
S_7	No damage	14.21
S_8	Mini cracks	15.24

Table 4 Data scenarios for noise-contaminated EMI scenarios

Scenario	Data type		
	Training set	Validation set	Testing set
Measured signal	16	8	8
Noise-contaminated signal	384	8	1288

To construct the training set, the Gaussian noise with standard deviations ranging from 0% to 5% of the signal amplitude was applied to the first two ensembles (among four ensembles), resulting in a total of 384 signals for 8 stress levels. The third ensemble was utilized to construct the validation set, and the total 8 signals were utilized as the validation set. To create the testing dataset, different levels of noise were added, ranging from 1% to 16%, to the remaining raw signals at each stress level. For each noise level, 10 new signals were generated for each of the eight stress levels, resulting in a total of 1280 signals for the 16 noise levels. The testing dataset consisted of 1288 signals, including the original 8 raw EMI signals measured without noise. The number of measured and noise-contaminated signals are summarized in Table 4.

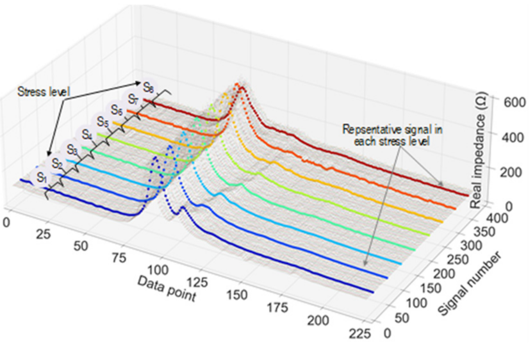

Fig. 12 Visualization of labeled data in training set

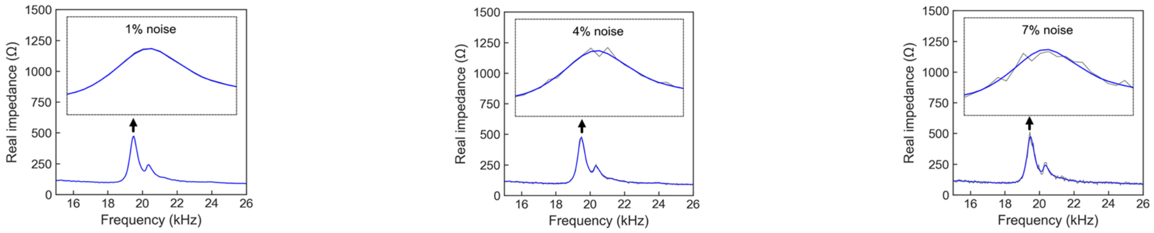

(a) 1% noise (b) 4% noise (c) 7% noise

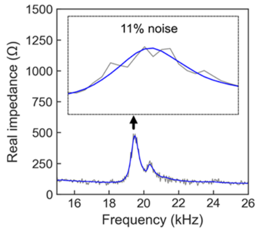

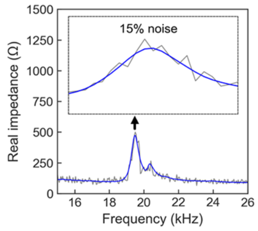

(d) 11% noise (e) 15% noise

Fig. 13 Example of noise-contaminated EMI signals under stress level S_1 in testing set

Fig. 12 visualizes the labeled EMI signals in the dataset for training the 2D CNN model. In the figure, each EMI signal was recorded with 225 data points. 10800 data points were recorded for each stress level. As a result, a total of 86400 data points were acquired for 8 stress levels. Fig. 13 illustrates examples of noise-contaminated EMI signals (under stress level S1 in the testing set. Note that total 16 levels of noise (1% ~ 16%) were added to the raw signals.

4.1.2 Training result

The computation of deep learning was conducted on a desktop computer equipped with a GPU (GeForce GT 2080 Ti, 11 GB), CPU (Intel Core i9-9000KF, 3.6 GHz), and 64 GB of RAM. The 2D CNN model was constructed using the Python programming language. The model was trained using the Adam optimizer algorithm with a mini-batch size value of 2 and a learning rate value of 0.0001.

Fig. 14 presents the loss values of the 2D CNN model after a training procedure of 100 epochs. The training and validation loss sharply dropped within the first five epochs, followed by a gradual convergence until the end. The 2D CNN model performed a convergence in loss values, indicating that the configuration of the 2D CNN model was designed effectively for learning and extracting optimal damage EMI features. The training time for 6067 parameters of 2D CNN was about 50.6 seconds. The trained2D CNN model at the 44th epoch, corresponding to the lowest loss validation value in the whole learning process, was selected to evaluate its accuracy on the testing set.

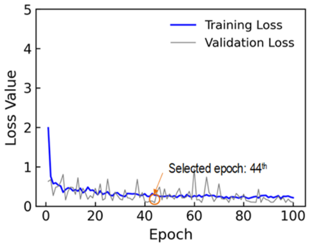

Fig. 14 Loss values of 2D CNN models after 100 epochs

4.1.3 Evaluation results

The effect of noise levels on the accuracy of the 2D CNN model for stress estimation is analyzed as shown in Fig. 15. In the figure, the estimated stress values were plotted against the actual stress values across different noise levels. At the 0% noise level, the model precisely estimated stress values with an RMSE error of approximately 0.07 (see Fig. 15(a)). At the 8% noise level, the model precisely predicted stress values with the RMSE error of about 0.49 (see Fig. 15(e)). It is observed that the estimation stress error of 2D CNN was over 30% at noise levels larger than 10%.

Fig. 16 shows linear relationships between various noise levels and RMSE values. As shown in Fig. 16(a), the RMSE was 0.07 at 0% noise level and 0.3 at 5% noise level. As shown in Fig. 16(b), the RMSE was 0.38 at 6.0% noise level and it was 1.03 at 16% noise level. It is observed that the RMSE values raised almost linear as the noise percentage from 0% to 5%. In general, the accuracy of stress estimation from the 2D CNN model decreased when the levels of noise increased. Thus, the empirical function of 2D CNN was encouraged to use for error estimation in practical applications.

4.2 Stress estimation for untrained stress-EMI scenarios

4.2.1 Data preparation

The databank of the untrained stress-EMI scenarios was formed by following the data configuration scheme described in Fig. 4. From the experiments, the EMI signals were recorded four times (four ensembles) for each applied stress level. Total 32 signals were obtained from stress levels S1- S8. The first two ensembles were used to establish the training set which produced a total of 384 signals for 8 stress levels. The third ensemble was used for the validation set which resulted in a total of 8 signals for

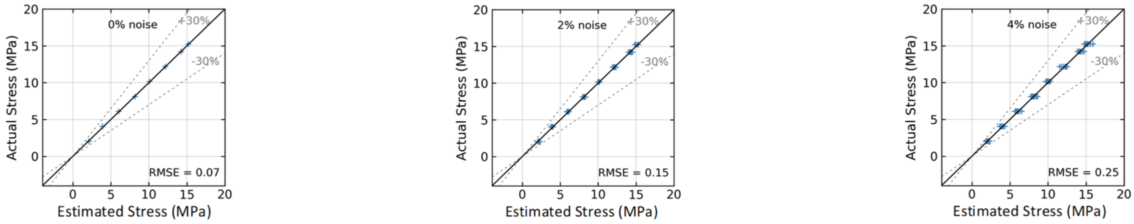

(a) 0% noise (b) 2% noise (c) 4% noise

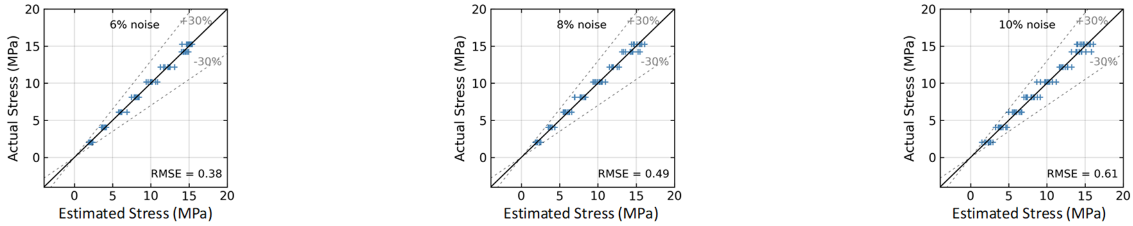

(d) 6% noise (e) 8% noise (f) 10% noise

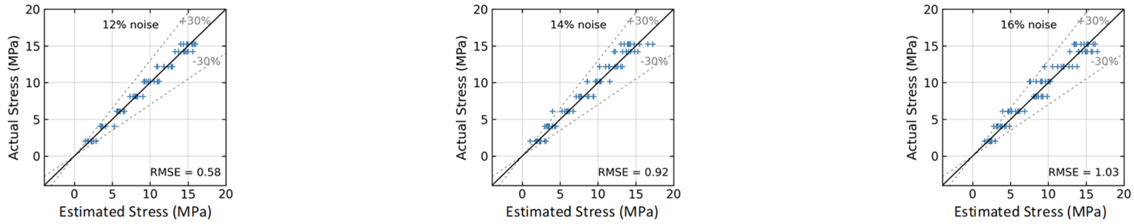

(g) 12% noise (h) 14% noise (e) 16% noise

Fig. 15 Stress estimation of 2D CNN model

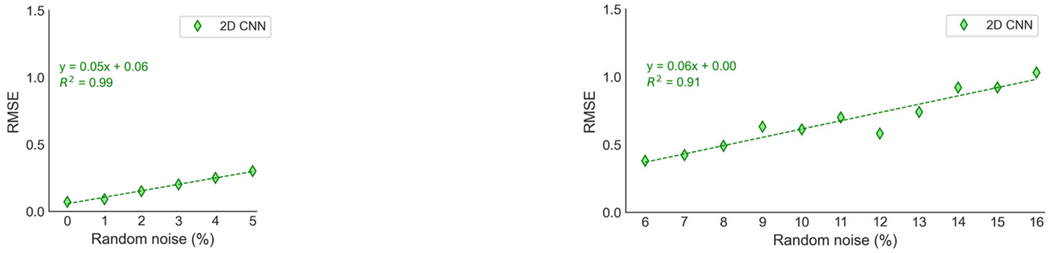

(a) Levels of noise 0%-5% (b) Levels of noise 6%-16%

Fig. 16 RMSE error of 2D CNN model under various noise levels

8 stress levels. The last ensemble was used to establish the testing set.

As summarized in Table 5, two scenarios were established to investigate the effect of untrained stress-EMI data on 2D CNN's performance. In the first scenario, the data for training and validating 2D CNN model were established by excluding the stress level S_2 (among eight levels S_1-S_8). 48 signals and 1 signal at stress level S_2 were excluded from the training and validation set, respectively. As a result, the remaining signals in the training set and validation set orderly were 336 signals and 7 signals. In the second scenario, the data for training and validating the model were established by excluding the stress levels S_2 and S_4. The 96 signals and 2 signals were excluded from the training and validation set, respectively. As a result, the remaining signals in the training set and validation set orderly were 288 signals and 6 signals.

Table 5 Data scenarios for untrained stress-EMI scenarios

Scenario	Data type		
	Training set	Validation set	Testing set
Untrained case 1	336	7	408
Untrained case 2	288	6	

Fig. 17 visualizes the labeled EMI data in the training set of the 2D CNN model under untrained scenarios. In the untrained scenario 1 (see Fig. 17(a)), the stress level S_2 was excluded from the training set. In the untrained scenario 2 (see Fig. 17(b)), the stress levels S_2 and S_4 were excluded from the training set.

4.2.2 Training result

Fig. 18(a) shows the loss values of the 2D CNN model during 100 epochs for the untrained scenario 1. In the figure, the training loss quickly dropped in the first 4 epochs

(a) Untrained scenario 1 (excluded stress S2) (b) Untrained scenario 2 (excluded stress S2, S4)

Fig. 17 Training data under untrained scenarios

(a) Scenarios 1 (excluded stress S2) (b) Scenarios 2 (excluded stress S2, S4)

Fig. 18 Loss values of 2D CNN model for untrained scenarios

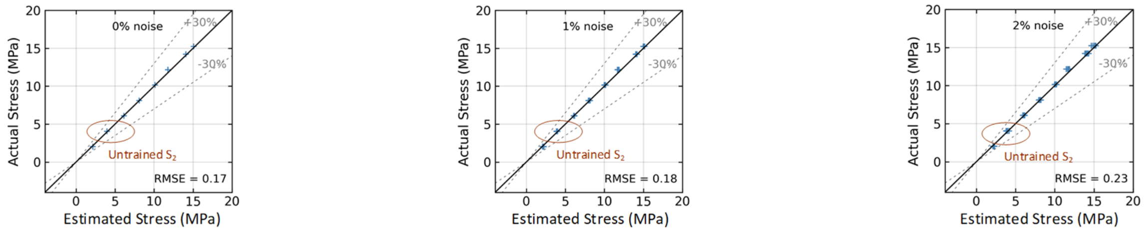

(a) 0% noise (b) 2% noise (c) 2% noise

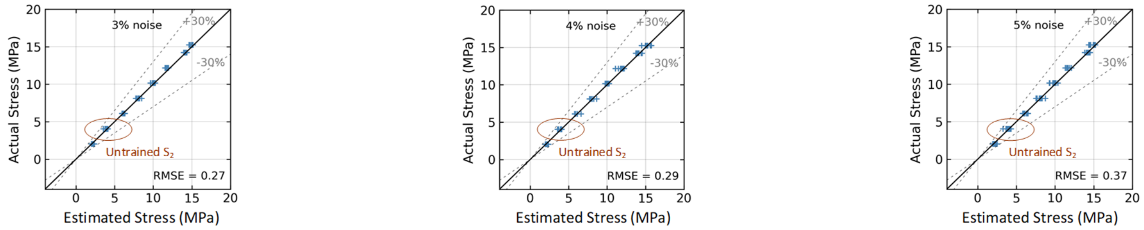

(d) 3% noise (e) 4% noise (f) 5% noise

Fig. 19 Stress estimation of 2D CNN model for untrained scenario 1 (excluded stress S2)

and then gradually decreased with minor fluctuations to the 100th epoch. The validation loss rapidly declined with high variations in the first 55 epochs. Afterward, the validation loss marginally fluctuated until the learning process's end. It is observed that the training loss value was approximately 0.21 at the 73rd epoch, corresponding to the lowest validation loss of nearly 0.06. Thus, the trained 2D CNN model at the 73rd epoch was selected to evaluate its accuracy on the testing set of untrained scenario 1.

Fig. 18(b) shows the loss values of the 2D CNN model during 100 epochs for the untrained scenario 2. In the figure, the training loss of 2D CNN rapidly decreased in the first 3 epochs. The loss continues to decline gradually with slight fluctuations until the 100 epoch. The validation loss showed a rapid decrease in the first 2 epochs. Afterward, the validation loss experienced fluctuations and reduction until the 100th epoch. It is observed that the minimum value of the validation loss was 0.06 at the 68th epoch with respect to the training loss value was about 0.22. Thus, the trained 2D CNN model at 68th epoch was selected to evaluate its accuracy on the testing set of untrained scenario 2.

4.2.3 Evaluation results

Fig. 19 shows the effect of untrained stress S_2 (untrained scenario 1) on the accuracy of the 2D CNN model. As shown in Fig. 19(a), with 0% noise level, the model precisely estimated stress with the RMSE error of approximately 0.17.

As shown in Fig. 19(e), with 4% noise level, the model accurately predicted stress with the RMSE error of approximately 0.29. Fig. 20 shows the effect of untrained stress levels S_2 and S_4 (untrained scenario 2) on the accuracy of the 2D CNN model. As shown in Fig. 20(a), with 0% noise level, the model predicted stress with the RMSE error of 0.2. As shown in Fig. 20(f), with 5% noise level, the model predicted stress with the RMSE error of approximately 0.38.

Fig. 21 shows the relationships between RMSE and noise levels. For untrained scenario 1 (see Fig. 21(a)), the RMSE accounted for 0.18 at 1% noise level and around 0.37 at 5% noise level. For untrained scenario 2 (see Fig. 21(b)), the RMSE accounted for 0.2 at 1% noise level and 0.31 at 4% noise level. Generally, when the amount of data in the training sets decreased, the accuracy of the 2D CNN model for stress estimation declined.

5. Comparative evaluation of 2D CNN and 1D CNN deep learning approaches for concrete stress estimation

5.1 Training performance

The training performance of 2D CNN and 1D CNN models was comparatively evaluated via the training set described previously in Section 4.1. As shown in Table 6, the training time of the 2D CNN model required 50.6 seconds for 6067 training parameters. The training time of the 1D CNN model took 64.5 seconds for 6081 training parameters. The 2D CNN model was constructed with 0.2% fewer training parameters and required 21.5% less training time than the 1D CNN model.

The loss values of 2D CNN and 1D CNN models was compared for a training process of 100 epochs, as shown in Fig. 22. The training loss values of both models experienced a downward trend (see Fig. 22(a)). The training loss values of 2D CNN model were slightly lower than 1D CNN model in the whole learning process. The validation loss values were also compared for the two models (see Fig. 22(b)). The validation loss values of 1D CNN highly fluctuated and continued larger fluctuation at the end, while that of 2D CNN has fluctuations with a trend of convergence.

5.2 Accuracy of stress estimation under noise-contaminated EMI scenarios

Fig. 23 presents an RMSE comparison between 2D CNN and 1D CNN models under noise levels. At 2% noise level (see Fig. 23(a)), RMSE of 2D CNN was 0.15 which was 37.5% lower than that of 1D CNN. At 5 % noise level, RMSE of 2D CNN raised to 0.3 which was 38.7% lower

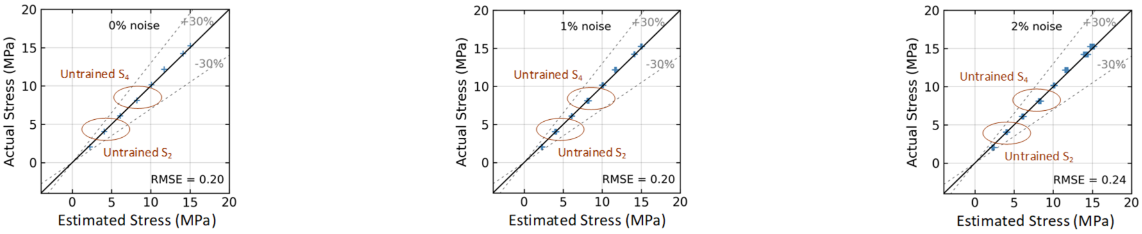

(a) 0% noise (b) 2% noise (c) 2% noise

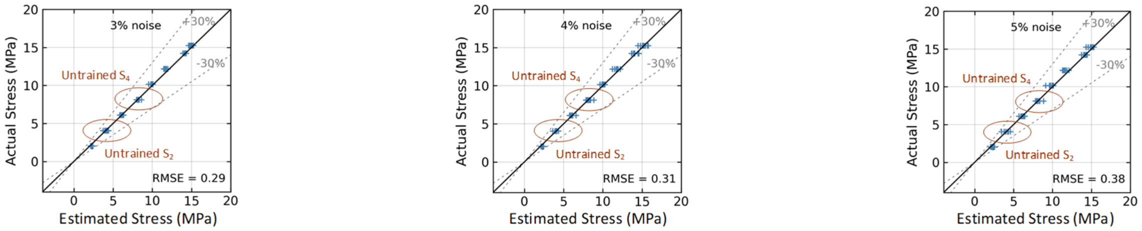

(d) 3% noise (e) 4% noise (f) 5% noise

Fig. 20 Stress estimation of 2D CNN model for untrained scenario 2 (excluded stress S_2, S_4)

(a) Scenarios 1 (excluded stress S_2) (b) Scenarios 2 (excluded stress S_2, S_4)

Fig. 21 RMSE error of 2D CNN model under untrained scenarios

(a) Scenarios 1 (excluded stress S_2)

(b) Scenarios 2 (excluded stress S_2, S_4)

Fig. 22 RMSE error of 2D CNN model under untrained scenarios

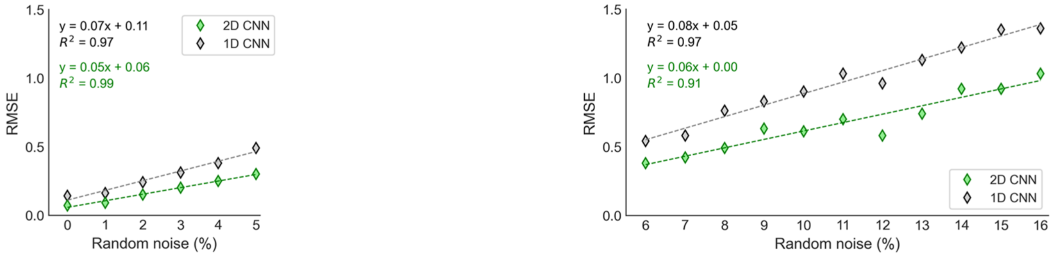

(a) Levels of noise 0%-5%

(b) Levels of noise 6%-16%

Fig. 23 RMSE comparison between 2D CNN and 1D CNN models under noise levels

(a) Scenarios 1 (excluded stress S_2)

(b) Scenarios 2 (excluded stress S_2, S_4)

Fig. 24 RMSE comparison of 2D CNN and 1D CNN models under untrained stress-EMI scenarios

Table 6 Comparison of training parameters and training time

	Model		Variation (%)
	2D CNN	1D CNN	
Training parameters	6067	6081	0.2
Training time (second)	50.6	64.5	21.5

than that of 1D CNN. As shown in Fig. 23(b), the RMSE of 2D CNN was 0.42 at 7% noise level which was 27.5% lower than that of 1D CNN. At a higher noise level of 15%, RMSE of 2D CNN achieved 0.92 which was 31.8% lower than that of 1D CNN.

5.3 Accuracy of stress estimation under untrained stress-EMI scenarios

Fig. 24 presents an RMSE comparison of 2D CNN and 1D CNN models under untrained stress-EMI scenarios. For the untrained scenario 1 (see Fig. 24(a)), RMSE of 2D CNN was 0.23 (21.1% higher than that of 1D CNN). At 5% noise level, RMSE of 2D CNN was 0.37 (24.4% lower than that of 1D CNN). For the untrained scenario 2 (see Fig. 24(b)), RMSE of 2D CNN was 0.24 at 2% noise level (27.3% lower than that of 1D CNN). At a noise level of 5%, RMSE of 2D CNN achieved 0.38 (17.4% lower than that of 1D CNN).

6. Conclusions

This study aimed to develop a 2D CNN deep learning of electromechanical impedance (EMI) from the capsule-like smart aggregate (CSA) sensor embedded in the concrete structure. The EMI measurement model was designed and theoretically described for the CSA-embedded concrete structure under compressive stress. The 2D CNN model was developed to learn CSA's EMI signals to estimate stress status in the concrete structures. The feasibility of the developed models was further investigated under the effect of noise-contaminated data and untrained data.

From the results, at least three major findings could be made as follows:

(1) The developed 2D CNN deep learning model effectively extracted damage features from raw EMI

signals provided by the CSA sensor. The model autonomously processed the signals and precisely estimated concrete stress values in the MPa unit.

(2) The accuracy of stress estimation from the 2D CNN model was significantly affected by noises injected into CSA's EMI signals. The accuracy of the 2D CNN model was decreased when levels of applied stress were excluded from the training data sets.

(3) In comparison with the previously established 1D CNN model (Ta *et al*. 2024a), the 2D CNN model not only achieved faster training time but also estimated concrete stress with lower errors, making it a promising option for realistic stress monitoring in field concrete structures.

Although promising results have been found, additional research is still needed: (1) Investigating the adaptability of the methodology for various stress types and proportions of concrete mixture. Also, implementing knowledge transfer learning techniques to efficiently retrain the 2D CNN model for other applications of concrete SHM; (2) Fine-tuning the hyperparameters and convolution kernels of the 2D CNN model using optimization methods to enhance its ability in estimating concrete stress in test specimens; (3) developing deep regression and classification learning methods for autonomous damage monitoring in concrete structures.

Acknowledgments

This work was supported by the Basic Science Research Program through the National Research Foundation of Korea. (2022R1A2C10038891161782064340101).

References

Abdeljaber, O., Avci, O., Kiranyaz, M.S., Boashash, B., Sodano, H. and Inman, D.J. (2018), "1-D CNNs for structural damage detection: Verification on a structural health monitoring benchmark data", *Neurocomputing*, **275**, 1308-1317. https://doi.org/10.1016/j.neucom.2017.09.069

Ai, D., Mo, F., Han, Y. and Wen, J. (2022), "Automated identification of compressive stress and damage in concrete specimen using convolutional neural network learned electromechanical admittance", *Eng. Struct.*, **259**, p. 114176. https://doi.org/10.1016/j.engstruct.2022.114176

De Oliveira, M.A., Monteiro, A.V. and Vieira Filho, J. (2018), "A new structural health monitoring strategy based on PZT sensors and convolutional neural network", *Sensors* (*Basel*), **18**(9), p. 2955. https://doi.org/10.3390/s18092955

Goodfellow, I., Bengio, Y. and Courville, A. (2016), *Deep Learning*, MIT Press.

Jalloh, A. (2005), "Effects of piezoelectric (PZT) sensor bonding and the characteristics of the host structure on impedance based structural health monitoring", The NASA Faculty Fellowship Program Research Reports.

Khan, M.K.I., Lee, C.K., Zhang, Y.X. and Rana, M.M. (2020), "Compressive behaviour of ECC confined concrete partially encased steel composite columns using high strength steel", *Constr. Build. Mater.*, **265**, p. 120783. https://doi.org/10.1016/j.conbuildmat.2020.120783

Kocherla, A., Duddi, M. and Subramaniam, K.V.L. (2021), "Embedded PZT sensors for monitoring formation and crack opening in concrete structures", *Measurement*, **182**, p. 109698. https://doi.org/10.1016/j.measurement.2021.109698

Lecun, Y., Bottou, L., Bengio, Y. and Haffner, P. (1998), "Gradient-based learning applied to document recognition", *Proceedings of the IEEE*, **86**(11), 2278-2324. https://doi.org/10.1109/5.726791

Lee, S.J., Ahn, D., You, I., Yoo, D.Y. and Kang, Y.S. (2020), "Wireless cement-based sensor for self-monitoring of railway concrete infrastructures", *Automat. Constr.*, **119**, p. 103323. https://doi.org/10.1016/j.autcon.2020.103323

Li, G., Luo, M., Huang, J. and Li, W. (2023), "Early-age concrete strength monitoring using smart aggregate based on electromechanical impedance and machine learning", *Mech. Syst. Signal Process.*, **186**, p. 109865. https://doi.org/10.1016/j.ymssp.2022.109865

Liang, C., Sun, F.P. and Rogers, C.A. (1994), "Coupled electro-mechanical analysis of adaptive material systems-determination of the actuator power consumption and system energy transfer", *J. Intell. Mater. Syst. Struct.*, **8**(4), 335-343. https://doi.org/10.1177/1045389X9700800406

Lim, Y.Y., Kwong, K.Z., Liew, W.Y.H. and Soh, C.K. (2016), "Non-destructive concrete strength evaluation using smart piezoelectric transducer: a comparative study", *Smart Mater. Struct.*, **25**(8), p. 085021. https://doi.org/10.1088/0964-1726/25/8/085021

Lin, M., Chen, Q. and Yan, S. (2013), "Network in network", arXiv preprint arXiv:1312.4400.

Melville, J., Alguri, K.S., Deemer, C. and Harley, J.B. (2018), "Structural damage detection using deep learning of ultrasonic guided waves", In: *AIP Conference Proceedings*, **1949**(1). https://doi.org/10.1063/1.5031651

Min, J., Park, S. and Yun, C.B. (2010), "Impedance-based structural health monitoring using neural networks for autonomous frequency range selection", *Smart Mater. Struct.*, **19**(12), p. 125011. https://doi.org/10.1088/0964-1726/19/12/125011

Na, W.S. and Baek, J. (2018), "A review of the piezoelectric electromechanical impedance based structural health monitoring technique for engineering structures", *Sensors* (*Basel*), **18**(5), p. 1307. https://doi.org/10.3390/s18051307

Narayanan, A., Kocherla, A. and Subramaniam, K.V.L. (2018), "PZT sensor array for local and distributed measurements of localized cracking in concrete", *Smart Mater. Struct.*, **27**(7), p. 075049. https://doi.org/10.1088/1361-665X/aaca4d

Nguyen, T.T., Kim, J.T., Ta, Q.B., Ho, D.D., Phan, T.T.V. and Huynh, T.C. (2021), "Deep learning-based functional assessment of piezoelectric-based smart interface under various degradations", *Smart Struct. Syst., Int. J.*, **28**(1), 69-87. https://doi.org/10.12989/sss.2021.28.1.069

Nguyen, T.T., Tuong Vy Phan, T., Ho, D.D., Man Singh Pradhan, A. and Huynh, T.C. (2022), "Deep learning-based autonomous damage-sensitive feature extraction for impedance-based prestress monitoring", *Eng. Struct.*, **259**, p. 114172. https://doi.org/10.1016/j.engstruct.2022.114172

Nguyen, T.T., Ta, Q.B., Ho, D.D., Kim, J.T. and Huynh, T.C. (2023), "A method for automated bolt-loosening monitoring and assessment using impedance technique and deep learning", *Develop. Built Environ.*, **14**, p. 100122. https://doi.org/10.1016/j.dibe.2023.100122

Ong, C.W., Yang, Y., Naidu, A.S.K., Lu, Y. and Soh, C.K. (2002), "Application of the electromechanical impedance method for the identification of in-situ stress in structures", *Smart Structures, Devices, and Systems*, Vol. 4935, pp. 503-514. https://doi.org/10.1117/12.485621

Park, G., Sohn, H., Farrar, C.R. and Inman, D.J. (2003), "Overview of piezoelectric impedance-based health monitoring and path forward", *Shock Vib. Digest*, **35**(6), 451-464.

Pham, Q.Q., Dang, N.L. and Kim, J.T. (2021a), “Piezoelectric sensor-embedded smart rock for damage monitoring in a prestressed anchorage zone”, *Sensors* (*Basel*), **21**(2), p. 353. https://doi.org/10.3390/s21020353

Pham, Q.Q., Dang, N.L., Ta, Q.B. and Kim, J.T. (2021b), “Optimal localization of smart aggregate sensor for concrete damage monitoring in PSC anchorage zone”, *Sensors*, **21**(19), p. 6337. https://doi.org/10.3390/s21196337

Pham, Q.Q., Ta, Q.B. and Kim, J.T. (2022), “Capsule-like Smart Aggregate with Pre-Determined Frequency Range for Impedance-Based Stress Monitoring”, *Sensors*, **23**(1), p. 434. https://doi.org/10.3390/s23010434

Pham, N.L., Ta, Q.B. and Kim, J.T. (2024), “Pseudo-damage simulation and CNN deep learning for damage identification of submerged structure-foundation systems”, *Struct. Health Monitor.*, **24**(4). https://doi.org/10.1177/14759217241288773

Pham, N.L., Ta, Q.B., Huynh, T.C. and Kim, J.T. (2025), “CNN federated learning for vibration-based damage identification of submerged structure-foundation system”, *J. Civil Struct. Health Monitor.*, pp. 1-26. https://doi.org/10.1007/s13349-025-00962-6

Salman, S. and Liu, X. (2019), “Overfitting mechanism and avoidance in deep neural networks”, arXiv preprint arXiv:1901.06566.

Smolana, A., Klemczak, B., Azenha, M. and Schlicke, D. (2021), “Experiences and analysis of the construction process of mass foundation slabs aimed at reducing the risk of early age cracks”, *J. Build. Eng.*, **44**, p. 102947. https://doi.org/10.1016/j.jobe.2021.102947

Song, G., Gu, H. and Mo, Y.L. (2008), “Smart aggregates: multi-functional sensors for concrete structures: a tutorial and a review”, *Smart Mater. Struct.*, **17**(3), p. 033001. https://doi.org/10.1088/0964-1726/17/3/033001

Sun, F.P., Chaudhry, Z., Liang, C. and Rogers, C. (1995), “Truss structure integrity identification using PZT sensor-actuator”, *J. Intell. Mater. Syst.*, **6**(1), 134-139. https://doi.org/10.1177/1045389X9500600117

Sun, L., Ma, Q., Han, F., Liu, Z., Li, J., Wang, P., Zhao, H. and Sun, J. (2020), “Experimental investigation on axial compression behavior of steel reinforced concrete columns with welded stirrups”, *Eng. Struct.*, **208**, p. 109924. https://doi.org/10.1016/j.engstruct.2019.109924

Suzuki, T., Shiotani, T. and Ohtsu, M. (2017), “Evaluation of cracking damage in freeze-thawed concrete using acoustic emission and X-ray CT image”, *Constr. Build. Mater.*, **136**, 619-626. https://doi.org/10.1016/j.conbuildmat.2016.09.013

Ta, Q.B., Pham, Q.Q., Pham, N.L., Huynh, T.C. and Kim, J.T. (2024a), “Smart aggregate-based concrete stress monitoring via 1D CNN deep learning of raw impedance signals”, *Struct. Control Health Monitor.*, **2024**(1), p. 5822653. https://doi.org/10.1155/2024/5822653

Ta, Q.B., Pham, Q.Q., Pham, N.L. and Kim, J.T. (2024b), “Integrating the capsule-like smart aggregate-based EMI technique with deep learning for stress assessment in concrete”, *Sensors*, **24**(14), p. 4738. https://doi.org/10.3390/s24144738

Ta, Q.B., Pham, N.L. and Kim, J.T. (2024c), “Integrated estimation of stress and damage in concrete structure using 2D convolutional neural network model learned impedance responses of capsule-like smart aggregate sensor”, *Sensors*, **24**(20), p. 6652. https://doi.org/10.3390/s24206652

Tan, X., Abu-Obeidah, A., Bao, Y., Nassif, H. and Nasreddine, W. (2021), “Measurement and visualization of strains and cracks in CFRP post-tensioned fiber reinforced concrete beams using distributed fiber optic sensors”, *Automat. Constr.*, **124**, p. 103604. https://doi.org/10.1016/j.autcon.2021.103604

Yuan, F.-G., Zargar, S.A., Chen, Q. and Wang, S. (2020), “Machine learning for structural health monitoring: challenges and opportunities”, *Sensors Smart Structures Technologies for Civil, Mechanical, Aerospace Systems 2020*, Vol. 11379, p. 1137903. https://doi.org/10.1117/12.2561610

Zagrai, A.N. and Giurgiutiu, V. (2001), “Electro-mechanical impedance method for crack detection in thin plates”, *J. Intell. Mater. Syst. Struct.*, **12**(10), 709-718. https://doi.org/10.1177/104538901320560355

Zhang, Y. and Wallace, B. (2015), “A sensitivity analysis of (and practitioners’ guide to) convolutional neural networks for sentence classification”, arXiv preprint arXiv:03820. https://doi.org/10.48550/arXiv.1510.03820

Appendix A: Comparison of 2D CNN architectures

A preliminary study was conducted to select a proper 2D CNN architecture for concrete stress monitoring. Three architectures M1, M2 and M3 were built based on the pre-existing 2D CNN architecture (Ta *et al*. 2024a). Then, the training performance of the architectures was evaluated comparatively using the training set in Section 4.1.

The layer properties of three architectures M1, M2, and M3 are presented in Table A1. Three architectures were built with varying depths, while the input and output layers of the three models were designed to be similar. The architecture M1 was constructed with a convolution layer (Conv1) with a ReLu activation function. The Maxpool1 and GAP layers orderly follow the Conv1 layer. A Fc layer was configured after the GAP layer. The architecture M2 was constructed by adding a convolution layer (Conv2) with a ReLu layer after the Conv1 layer of M1. The added layers could increase the data's non-linear transformations and enhance the training procedure's convergence speed (Zhang and Wallace 2015). The architecture of M3 was built by increasing the depth of M2. All convolutional layers were set for the same padding. The layer properties of each architecture regarding the type, depth, filters, stride, and padding are described in Table A1.

Table A1 Layer properties of the three 2D CNN architectures (M1−M3)

Model M1					
Layer	Type	Depth	Filter	Stride	Padding
1	Conv1 + ReLu	18	3 × 3	1	Same
2	Maxpool1	-	2 × 2	2	-
3	GAP	-	-	-	-
4	Fc1	1	-	-	-
5	Regression	-	-	-	-
Model M2					
1	Conv1 + ReLu	18	3 × 3	1	Same
2	Conv2 + ReLu	18	3 × 3	1	Same
3	Maxpool1	-	2 × 2	2	-
4	GAP	-	-	-	-
5	Fc1	1	-	-	-
6	Regression	-	-	-	-
Model M3 (see Table 1)					

The training and validation loss values of the architectures M1, M2, and M3 during a learning process of 100 epochs are shown in Figure A1. As seen in the figures, the loss values of training and validation dropped in the 100 epochs and converged until the last epoch. Among the three architectures, M3 had the lowest loss during learning, followed by M2 and then M1. For a learning process of 100 epoch, the M3 architecture exhibited the highest performance in efficiently extracting optimal features from EMI data sets. As a result, the M3 architecture was chosen for the concrete stress estimation model.

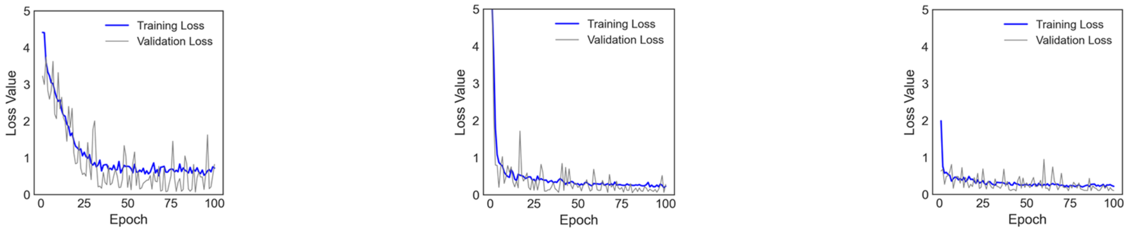

(a) M1 (b) M2 (c) M3

Fig. A1 Training and validation loss of three 2D CNN architectures (M1 – M3)